Journal of Materials Chemistry A

Accepted Manuscript

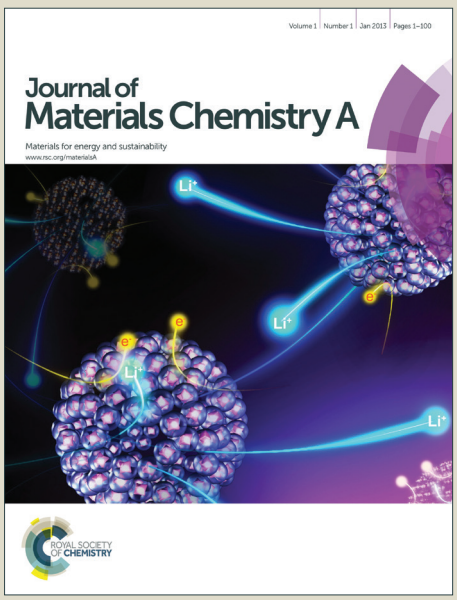

ROYAL SOCIETY OF CHEMISTRY

www.rsc.org/materialsA

High temperature humidity sensors based on WO_3/SnO_2 composite hollow nanospheres

Han Li,[1] Bin Liu,[1] Daoping Cai,[1] Yanrong Wang,[1] Yuan Liu,[1] Lin Mei,[2] Lingling Wang,[1] Dandan Wang,[1] Qiuhong Li[1] and Taihong Wang*[1]

[1]Pen-Tung Sah Institute of Micro-Nano Science and Technology, Xiamen University, Xiamen, China. E-mail: thwang@xmu.edu.cn; Fax: +86-0592-2187196; Tel: +86-0592-2183063

[2]Key Laboratory for Micro-Nano Optoelectronic Devices of Ministry of Education, State Key Laboratory for Chemo/Biosensing and Chemometrics, Hunan University, Changsha, China.

Abstract: Three kinds of humidity sensors were fabricated from WO_3/SnO_2 composite hollow nanospheres (WO_3-SnO_2 HNS), WO_3 nanoparticles (WO_3 NPs) and SnO_2 nanoparticles (SnO_2 NPs). WO_3-SnO_2 HNS were prepared by a facial hydrothermal process with diameter and thickness of about 550nm and 30nm. Temperature dependent properties of as-prepared humidity sensors was investigated at various values of relative humidity and temperature. It was found that WO_3-SnO_2 HNS humidity sensor showed good performance at 80℃. As the humidity switched between 35 RH% and 98% , the response time decreased from 289 to 29s, the recovery time reduced from 22 to 8s, and the sensitivity changed from 16.2 to 11.4 as the work temperature was raised from 24 to 80℃. Opposite humidity sensing phenomenon was observed between WO_3 NPs and SnO_2 NPs at high temperature, which might give the explanation to the temperature dependent properties of WO_3-SnO_2 HNS humidity sensor. This work could stimulate a right approach to design practical humidity sensors with high sensitivity, long stability and fast response.

1 Introduction

Humidity sensing plays an important role in daily life involving many areas, such as environmental moisture, automotive, medical, semiconductor, meteorological and food processing industries [1-2]. Nanostructure metal oxides have been used as common selective for the construction of humidity sensors due to their much superiority in stability avoiding degradation, high response and broad range of operation [3-6]. Although many oxides have been investigated for humidity sensor development, further research is still requested to optimize the sensor characteristics, e.g. sensitivity, low hysteresis, excellent stability and short response/recovery times [7]. Many semiconductor hetero-contact system, such as TiO_2/ZnO [7], TiO_2/SnO_2 [8], TiO_2/Al-doped ZnO [9], and ZrO/SnO_2 [10], were reported to have enhanced sensitivity and less hysteresis than pure components since one material is responsible for fast adsorption, and the other for fast desorption. Nevertheless, to the best of our knowledge, almost all ceramic materials humidity sensors researched at present work in the condition of room temperature. Thus water vapor adsorbed on the materials surface cannot be completely desorbed inevitably, which gives rise to the hysteresis and instability. An integral heater is frequently required to periodically regenerate ceramic sensors and recover the humidity-sensitive properties that characterize the virgin sensor[11]. In addition, in many cases, for instance, industrial drying, food processing, metallurgical process and high temperature operating machines, humidity sensors working at high temperature are in demand.

SnO_2 is a versatile semiconductor material which is commonly used for gas sensors and has a good sensitivity to relative humidity at low temperature [12-14]. On the other hand, owing to its distinctive properties, WO_3 have been used to construct ‘smart-window’, anti-glare rear view mirrors of automobiles, non-emissive displays, optical

recording devices, solid-state gas sensors, humidity and temperature sensors, biosensors, photonic crystals and so forth [15]. And WO_3 was reported to have high hydrophilic properties among metal oxides [16], and has been widely investigated as humidity sensors [17-18]. Therefore, their combination is expected to exhibit novel properties implementing in gas sensors, such as tunable sensitivity and wide operating temperature range. Ling and Leach have reported that even at 300℃, relative humidity has effect on the sensitivity of gas sensor based on WO_3/SnO_2 heterojunction [19]. And tungsten oxide-tin oxide nanocomposites have also been prepared to research the gas sensing properties of NO2 and ethylene [20-21], but the fabrication process is complicated and harsh.

In this work, we fabricated WO_3-SnO_2 HNS using a simple one-step hydrothermal reaction. More interestingly, the nanomaterials obtained after annealing have hollow structure which is required for gas sensors, and many researches about the superior gas sensing properties of hollow structure have been reported [22-24]. Because hollow micro/nanospheres exhibit an advantage to accomplish both high sensitivity and fast response because of high surface areas, low density, good permeation, and less agglomerated configurations [25]. The humidity sensor based on WO_3-SnO_2 HNS exhibited excellent humidity activity in contrast to pure SnO_2 and WO_3 NPs synthesized using the same method. In spite of this, the temperature dependent properties of humidity sensors were researched. Comparing with the characteristics at room temperature, better humidity properties of WO_3-SnO_2 HNS at high temperature was demonstrated. This work will pave a way to develop promising practical humidity sensors.

2 Experimental details

2.1 synthesis of materials

WO_3-SnO_2 HNS were synthesized using a facial hydrothermal method followed by calcination. In a typical experiment, 1mmol Na_2WO_4 was put into 50mL of deionized water under stirring to form a homogeneous solution. Subsequently, 0.5mmol Na_2SnO_3 and 5g glucose were introduced into the above homogeneous solution under continuous stirring for several minutes. Afterwards, the homogeneous solution was transferred into a Teflon-lined stainless steel autoclave with a capacity of 100mL. Then the autoclave was sealed and heated in an oven at 200℃ for 20h. After naturally cooling to room temperature, the solid products were subjected centrifugation, washed with distilled water and ethanol for several times, and finally dried in air at 60℃. In the next step, the as-prepared dry products were annealed in Muffle furnace at 500℃ for 2h in air. SnO_2 NPs and WO_3 NPs were prepared for comparison using the same method. For preparation of SnO_2 NPs, 1.5mmol Na_2SnO_3 and 5g glucose were added into 50mL deionized water to form a homogeneous solution under stirring, and then the products were obtained by following the above steps. And to obtain WO_3 NPs, 1.5mmol Na_2WO_4 and 5g glucose were required.

2.2 Characterization of materials

X-ray powder diffraction (XRD) data of the as synthesized materials were collected on a Philips X'pert pro diffractometer using Cu-Kα radiation at 40kV and 30mA. Scanning electron microscopy (SEM) images were recorded on Hitachi S4800 scanning electron microscope. The transmission electron microscopy images (TEM) and energy dispersive spectra (EDS) were performed on JEOL JEM-2100.

2.3 Fabrication and measurement of humidity sensors

The humidity sensors were fabricated through the procedures similar to the fabrication method of general gas sensors [26]. The schematic diagram of the humidity sensors is shown as Fig. 1. In a typical way, small amount of sensor material powder was mixed with terpineol to form a paste and then coated uniformly onto the outside surface of an alumina tube. A small Ni-Cr alloy coil was placed through the tube as a heating resistor which could

supply the operating temperature as high as 500℃. Electrical contacts were made with two Pt wires attached to each gold electrode. The various humidity environment was obtained by LiCl, NaBr, NaCl, KCl, and K_2SO_4 saturated solution. Those saturated solution were corresponding to about 11%, 59%, 75%, 85%, and 98% RH, respectively. The sensitivity is defined as $(S = R_{RH} / R_{air}, R_{RH} > R_{air})$ or $(S = R_{air} / R_{RH}, R_{air} > R_{RH})$, where R_{RH} and R_{air} denotes the resistance of the sensors in detecting humidity environments and air, respectively. The response time is defined here as the time required for 90% increment in conductance when the humidity sensors are introduced into the specified humidity environment from the air. The circumstances humidity was about 35%, and the temperature was 24℃. The response of the humidity sensors was measured through monitoring the variation of the DC conductance.

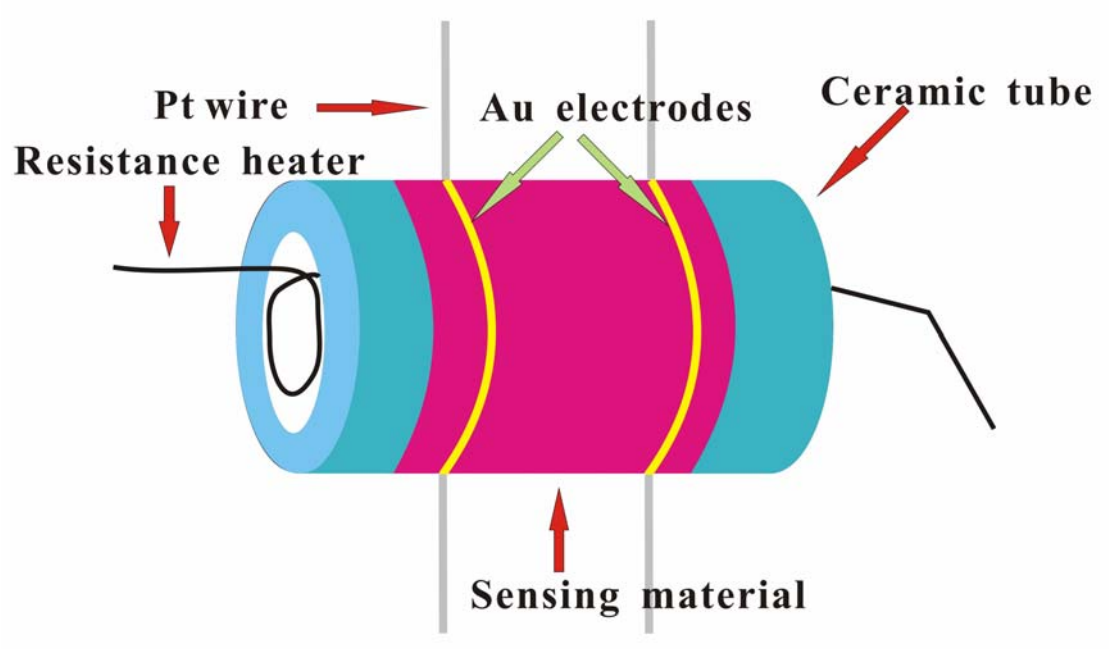

Fig. 1 Schematic illustration of the humidity sensors.

3 Results and discussion

Figure 2 shows the XRD patterns of the as synthesized WO_3-SnO_2 HNS, SnO_2 NPs and WO_3 NPs. All diffraction peaks of the lower XRD pattern can be indexed as Tetragonal SnO_2, indicating high purity of the products. Similarly, the middle XRD pattern well coincides with Monoclinic WO_3. And the uppermost XRD pattern corresponds to the WO_3-SnO_2 composites. It can be observed that all the peaks of the composites can be found in the Monoclinic WO_3 and Tetragonal SnO_2 XRD patterns, moreover, it preserve all the peaks of Tetragonal SnO_2 and the highest three peaks of Monoclinic WO_3. This agreement of XRD patterns can be attributed to the same synthesis conditions of the single component nanomaterials and the nanocomposites.

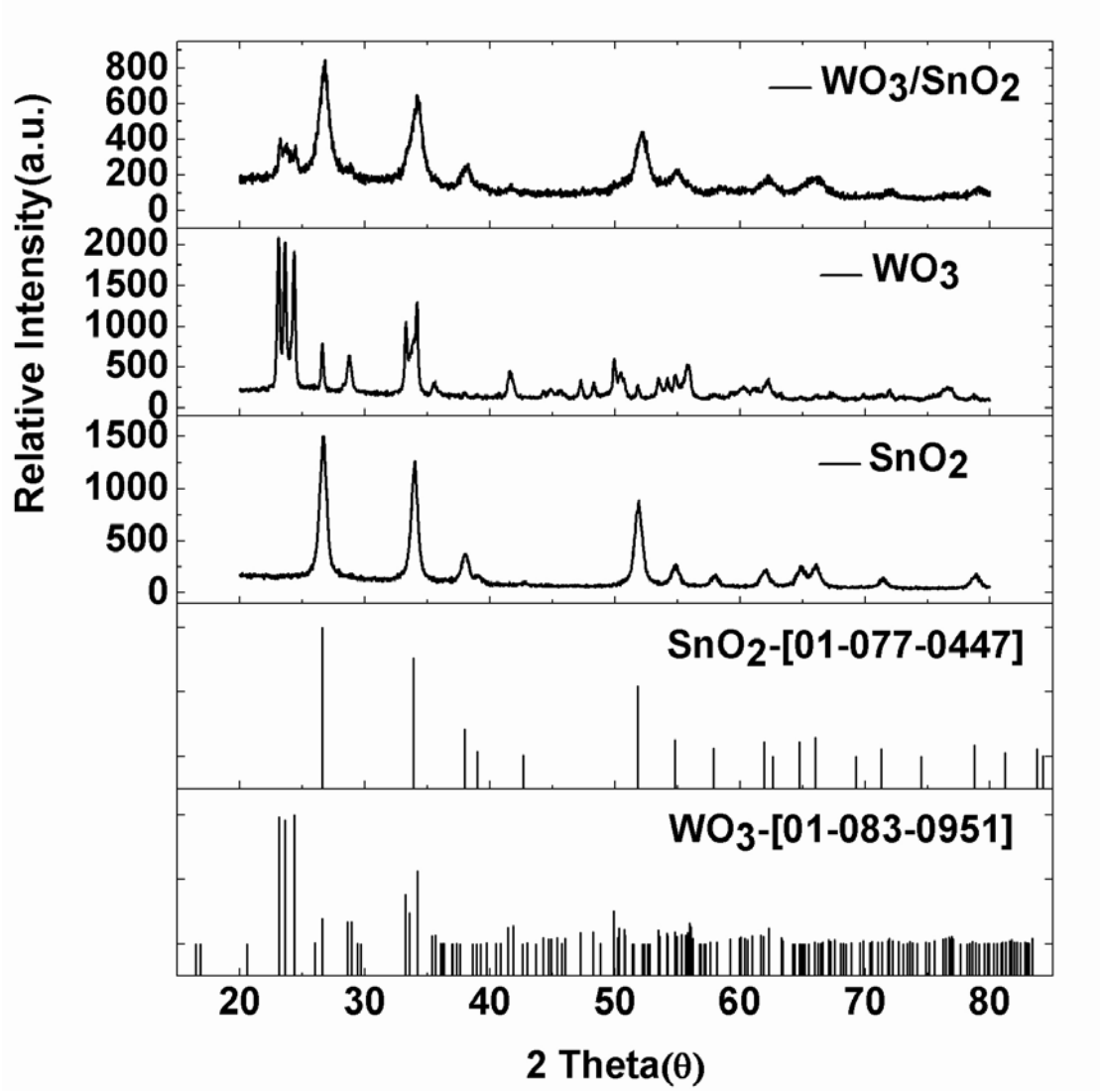

Fig. 2 XRD patterns of SnO_2 NPs , WO_3 NPs and WO_3/SnO_2 HNS (references from ICDD database).

The morphology and structure of as-prepared products were investigated by SEM. The overall morphology of WO_3-SnO_2 HNS is showed in Fig.3a, indicating that the samples is composed of abundant nanospheres with good monodispersity, and all nanospheres are roughly uniform and spherical. More details can be seen in high magnification image, the hollow spheres are composed of many small crystal particles assembled together, and the average diameters of the spheres is about 550nm, as shown in Fig. 3b. SEM observation also gives some sight to the broken sites and exposed hollow interiors of the nanospheres, which provide direct evidence that the nanospheres have a hollow structure. Fig. 3c and Fig. 3d present typical SEM images of as-synthesized SnO_2 NPs with diameters ranging from 15nm to 20nm. Morphology of WO_3 NPs is shown in Fig. 3e and Fig. 3f. It can be seen that WO_3 NPs with irregular size and shape aggregate heavily.

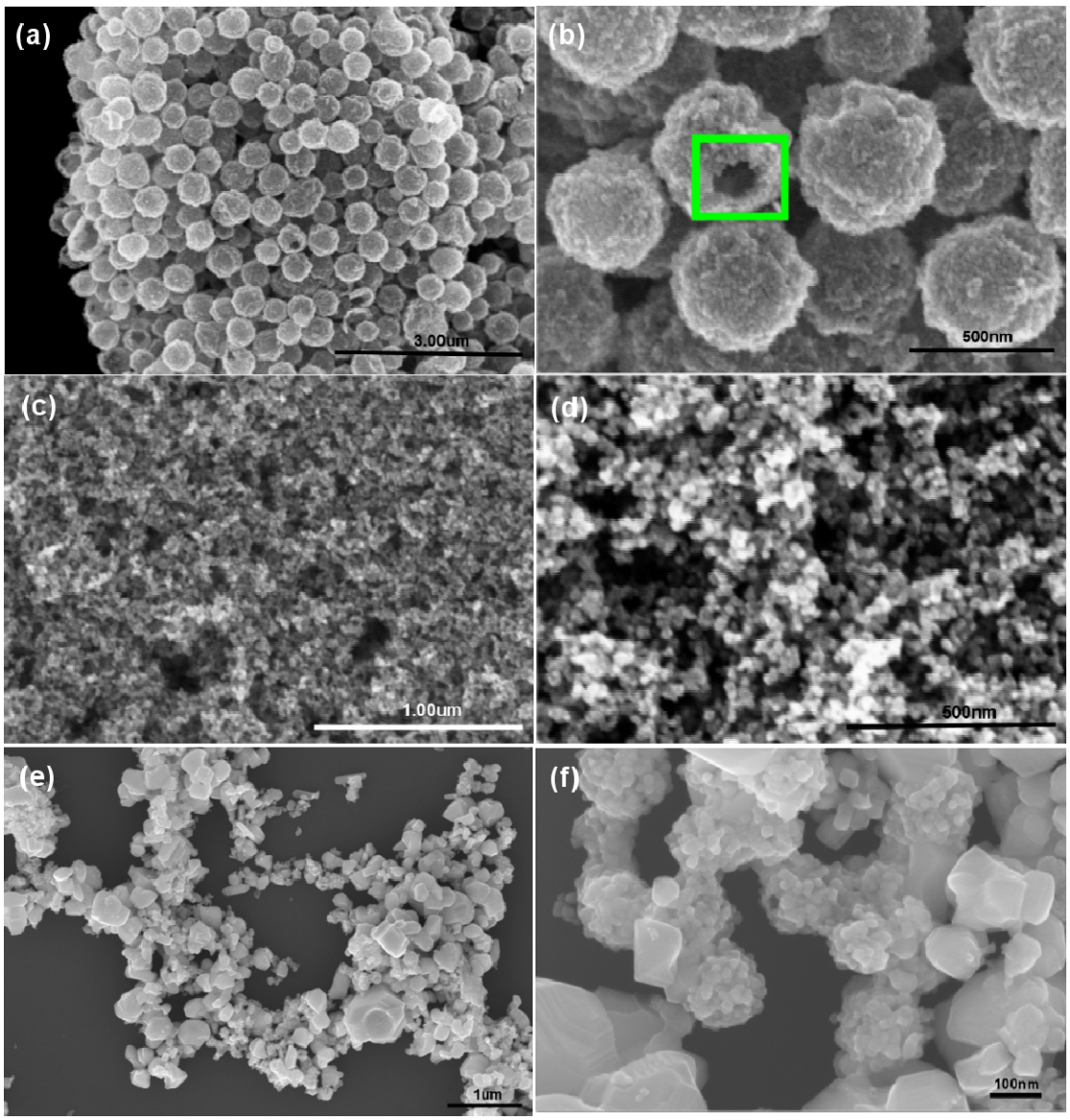

Fig. 3 (a) and (b) SEM images of WO_3-SnO_2 HNS. A small opening in the shell wall of a sphere has been indicated clearly. (c) and (d) SEM images of SnO_2 NPs. (e) and (f) SEM images of WO_3 NPs.

The hollow structure of WO_3-SnO_2 HNS was further investigated by TEM. Fig. 4a and Fig. 4b show the low and high magnification TEM images, respectively. Hollow interior of the nanospheres can be confirmed by the contrast between the dark edges and the pale center, as shown in Fig. 4a. As shown in Fig. 4b, rough surface of the nanospheres can be clearly observed, and many spots with clear contrast are observed in the central area, suggesting that hollow nanospheres consisted of primary nanocrystals. The corresponding SAED pattern (inset in Fig. 4b) conforms that the nanosoheres are polycrystalline structures in nature. The composition of the nanospheres was examined using an energy dispersive x-ray spectrometer (EDS). As shown in Fig. 4c, only three elements, O, W, and Sn, are identified in this spectrum. The high-resolution TEM (HRTEM) images shown in Fig. 4d and Fig. 4e indicate that the primary nanoparticles are highly crystalline. The lattice distances of 0.335nm and 0.342nm indicated in Fig. 4d agree with the (110) lattice plane of Tetragonal SnO_2 (0.335nm) while the lattice distance of 0.358nm marked in Fig. 4e correspond to the (200) crystalline plane of anorthic WO_3 (0.365nm). Fig. 5 shows the adsorption and desorption isotherms. The corresponding Brunauer-Emmett-Teller (BET) surface area is 49.850 m^2/g, and the average pore size is 1.42nm.

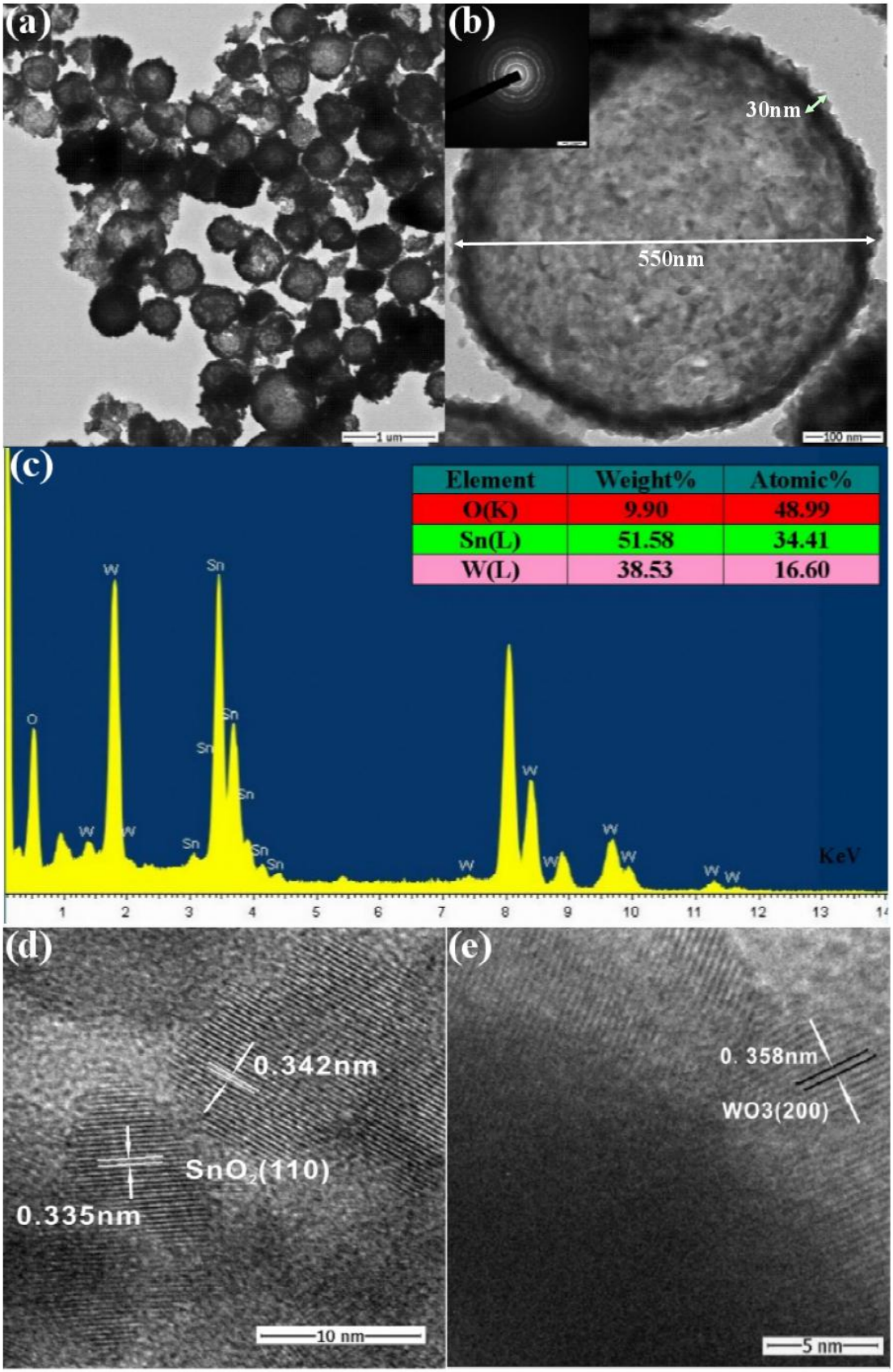

Fig. 4 (a) and (b) TEM images of WO_3-SnO_2 HNS. (c) EDS pattern of WO_3 -SnO_2 HNS. (d) and (e) HRTEM images corresponding to SnO_2 NPs and WO_3 NPs of the nanospheres, respectively.

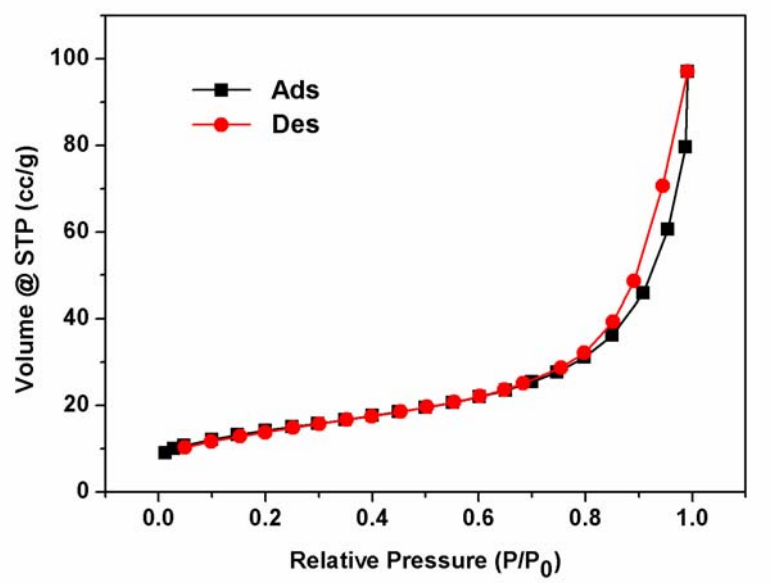

Fig. 5 Nitrogen adsorption and desorption isotherms for the WO_3/SnO_2 HNS.

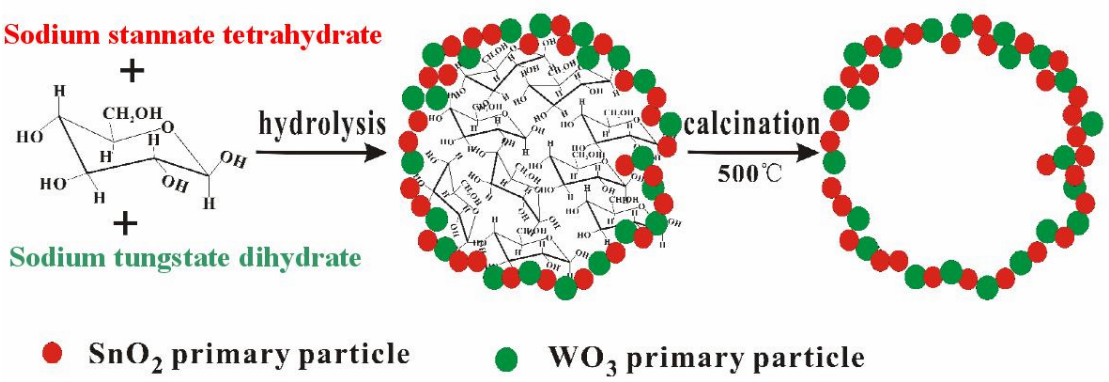

Fig. 6 Schematic illustrating the synthesis mechanism of WO_3/SnO_2 HNS.

The evolution of hollow nanospheres by self-assembly of the WO_3 and SnO_2 nanoparticles can be postulated as a schematic illustration displayed as Fig. 6 [27]. It can be recognized that both the WO_3 and SnO_2 precursors make contribution to the formation of the hollow structure since any one of them cannot achieve this effect using the same synthesis method. The formation mechanism of the hollow spheres products is likely associated with the properties that WO_3 hollow structures can be obtained by one-pot hydrothermal process when appropriate concentration Na_2WO_4 reacts with glucose at 200℃ [28]. And in this experiment, Na_2SnO_3 may controls the hydrolysis degree of Na_2WO_4 because of its alkaline. The influence of the concentration of Na_2SnO_3 on the morphology of nanocomposites was investigated. Fig. 7 shows SEM images and XRD pattern of nanocomposites synthesized by different amount of Na_2SnO_3 and 1mmol Na_2WO_4. As shown in Fig. 7a, when the reaction was carried out with 0.2mmol Na_2SnO_3, a small number of nanospheres coexist with irregular aggregates of nanoparticles. As the amount of Na_2SnO_3 was increased to 0.5mmol, the obtained product consisted of large scale nanospheres, as shown in Fig. 7b. However, aggregated particles without orderly shape were collected when the amount of Na_2SnO_3 increased to 1mmol, as shown in Fig. 7c. In addition, the crystal structure and composition of the products with different added amounts of Na_2SnO_3 were investigated by X-ray diffraction. It is to discover that

strong peaks of anorthic WO_3 appear when the added amount of Na_2SnO_3 is only 0.2mmol except the peaks of Tetragonal SnO_2. Interestingly, the characteristic peaks of Monoclinic WO_3 become weak with increasing the amount of Na_2SnO_3 to 0.5mmol, and nearly disappear when the amount of Na_2SnO_3 reaches to 1mmol, as shown in Fig. 7d. This regular phenomenon indicates that Na_2SnO_3 plays an important role in controlling the formation of WO_3.

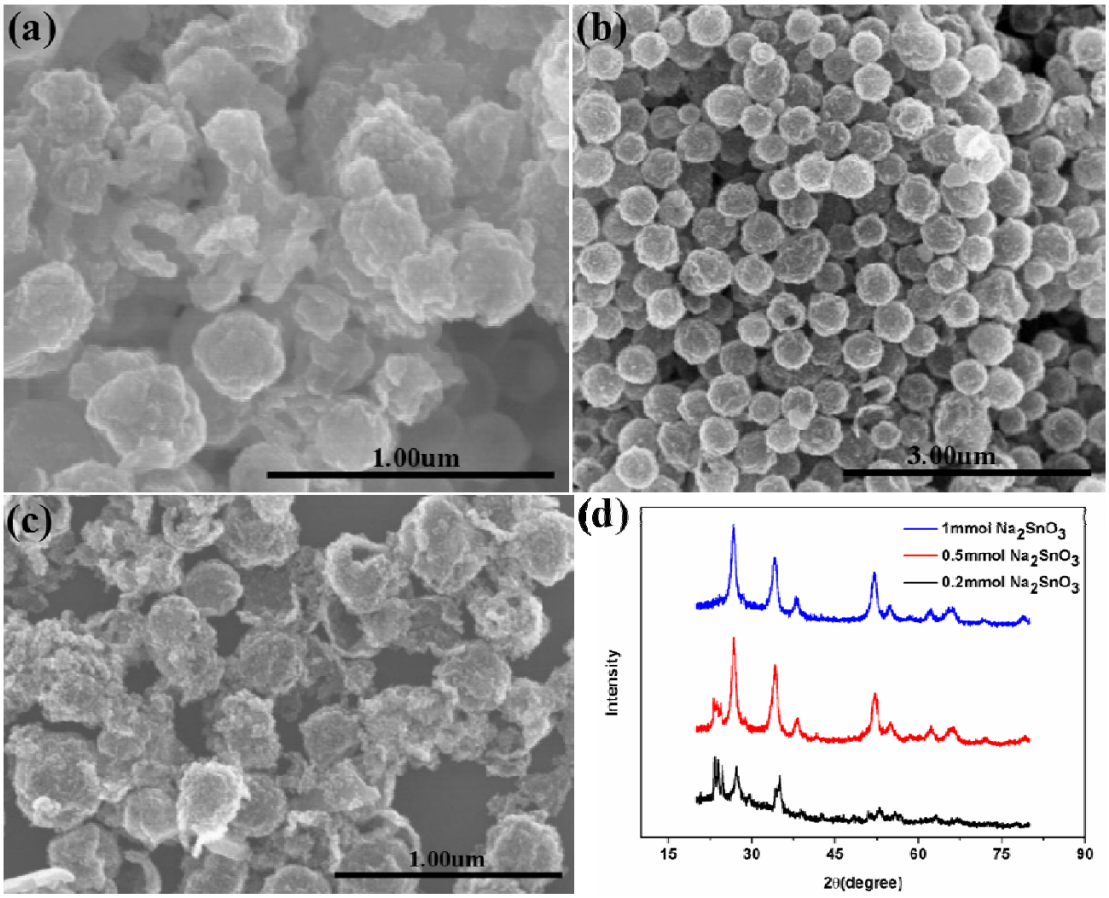

Fig. 7 SEM images and XRD patterns of WO_3-SnO_2 HNS nanocomposites with different added amounts of Na_2SnO_3. (a) 0.2mmol, (b) 0.5mmol, (c) 1mmol, (d) XRD patterns.

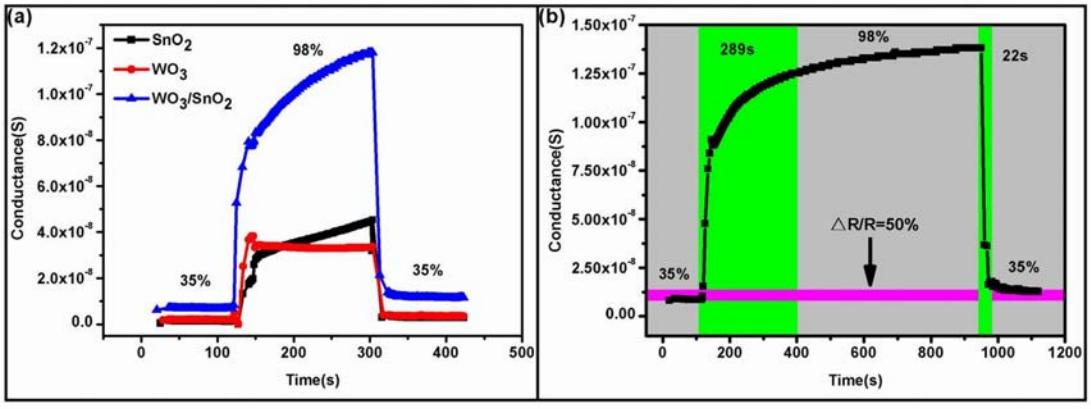

Fig. 8 Characteristics of the humidity sensors at room temperature. (a) Response and recovery of the three kind humidity sensors between the air (35% RH) and 98% RH. (b) Response and recovery of a typical humidity sensor based on WO_3-SnO_2 HNS.

Humidity sensing performance was measured in ambient air at room temperature with 35% RH. Response and recovery of three kinds of humidity sensors at 98% RH are shown in Fig. 8a. It was found that the conductance of the sensors increases gradually with the humidity increase. The sensor based on WO_3-SnO_2 HNS showed a higher sensitivity than the other two kinds of humidity sensors. The improved sensitivity was attributed to the more active sites provided by the high surface areas of hollow spheres [20, 25, 29]. However, the response time was 289s and recovery time was 22s, as shown in Fig. 8b. What was more, the equilibrium conductance of the humidity sensor when taken back to the air from humidity of 98% RH changes about 50% comparing with the initial conductance. The instability of humidity sensor resistance would cause deterioration of sensor accuracy. All this properties are determined by the sensing mechanism. At low temperature, when sensing material is exposed to humidity, water molecules can chemisorb on the available sites by forming hydrogen bonds with the oxygen atoms of the oxide surface. At low humidity, after the first layer of water molecules adsorbed on the surface, a dissociative mechanism leads to the formation of a hydroxyl ion (OH^-) and a proton (H^+) [18]. With increasing humidity, further physisorbed layers are formed, then H^+ ions can move freely in the physisorbed water according to the Grotthuss's chain reaction [30-31]. However, the adsorption and desorption of water molecules are slow processes at low temperature.

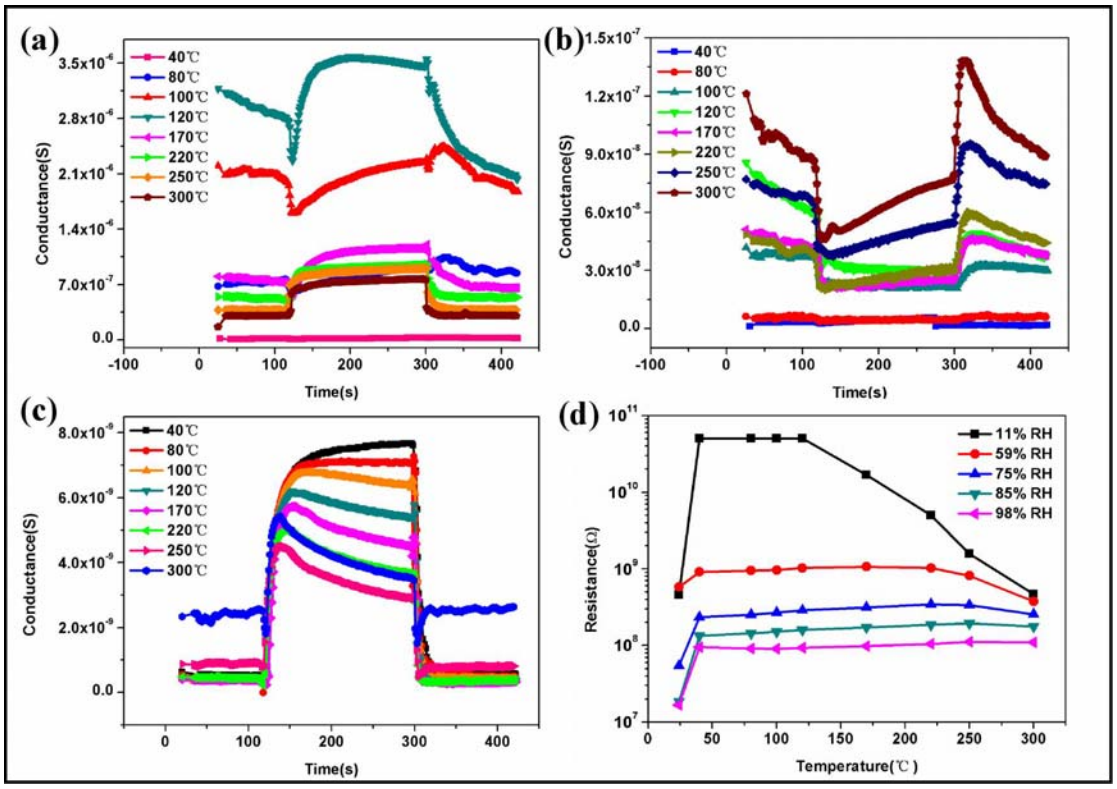

Fig. 9 Temperature dependent properties of the three kinds humidity sensors between air (35% RH) and 98% RH. (a) SnO_2 NPs (b) WO_3 NPs (c) WO_3-SnO_2 HNS. (d) Resistance variation characteristic of WO_3-SnO_2 HNS along with temperature in different RH.

To improve the humidity sensing properties, temperature dependent measurements were conducted. As the working temperature was raised from 24 to 40℃, either the SnO_2 sensors or the WO_3 sensors showed weak response to 98% RH, as shown in Fig. 9a and 9b. Such a behavior is in a good agreement with the reported results[32], which is mainly due to the fact that 40℃ is considered as the desorption temperature of physically adsorbed water on SnO_2. In contrast, the WO_3-SnO_2 HNS had a good performance at relative high temperature, and its optimum operating temperature was about 80℃, as shown in Fig. 9c. The improved performance can be

attributed to the large active area of hollow structure for gas adsorption. At a relative high temperature (40℃—100℃), the decrease of sensor resistance with increasing the RH is caused by competitive adsorption between H_2O and adsorbed oxygen species (O^{2-}, O^-, etc.) and desorption of the adsorbed oxygen species and releasing of free electrons [33], as illustrated in Fig. 10a.

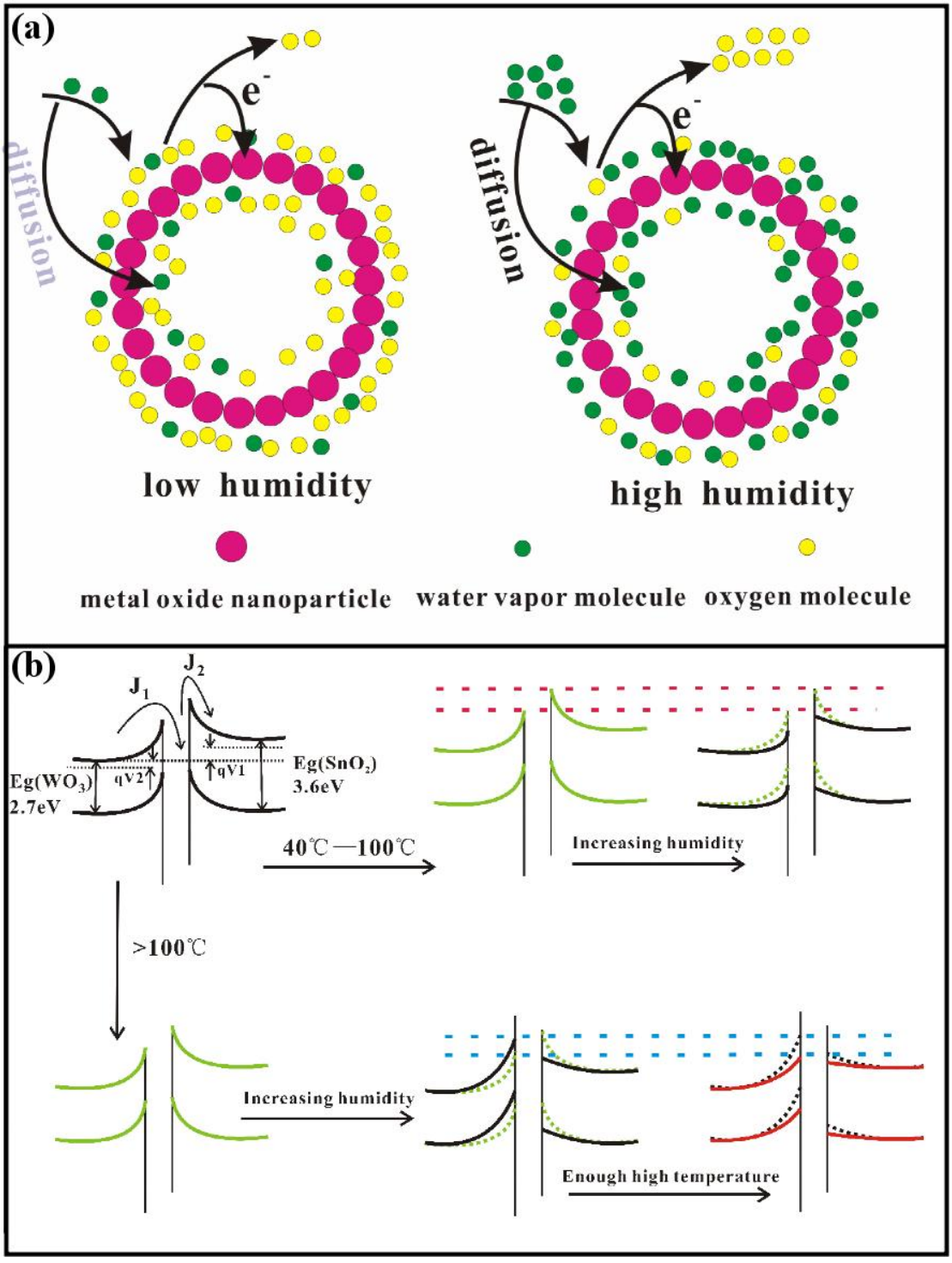

Fig. 10 Schematic of sensing mechanism of the WO_3-SnO_2 HNS humidity sensor. (a) H_2O molecules and oxygen species competitive adsorption model for humidity sensor working at high temperature. (b) Energy band structure of the WO_3/SnO_2 hetero-nanospheres in different temperature and humidity conditions.

With further raising the temperature above 100℃, the conductance of the SnO_2 NPs increases and the sensors exhibited stable response. A peak appeared in the conductance curve at 100℃ or 120℃. It is hard to explain what kind of physical-chemical change occurs on the surface, but it is thought that the peak response is caused by the adsorption or desorption of H_2O [33]. But the phenomenon was quite different for WO_3 NPs. At the temperature above 100℃, sensor conductance decreased with increasing RH, as shown in Fig. 9b. At high temperature (100-500℃), water molecules can react with the Lewis acid site (Sn) and Lewis base site (O) on the SnO_2 surface and then release electrons [13]. This probably accounts for the characteristic of SnO_2 NPs humidity sensor operating above 100℃. The mechanism can be described by [34]

$$H_2O^{gas} + Sn_{Sn} + O_O \Leftrightarrow (Sn_{Sn}{}^{\delta+} - OH^{\delta-}) + (OH)_O^+ + e^- . \quad (1)$$

And the opposite feature is suggested to be the result of catalytic reactions of gas phase water at the surface of WO_3 [15,35]. As shown in Fig. 11, in the catalytic reaction, water molecules firstly physically adsorb on W lattices, and then H^+ of the adsorbed water is reduced with decreasing the surface electron density of WO_3. With increasing RH, more water would be adsorbed on the oxygen vacancy site, and then be reduced, giving rise to a decrease of the conductance. And for WO_3-SnO_2 HNS humidity sensor, the sensitivity decreased with increasing the temperature, and the conductance gradually decreased in the 98% RH, as shown in Fig. 9c. Such a phenomenon could be explained by considering the combined effect of WO_3 and SnO_2.

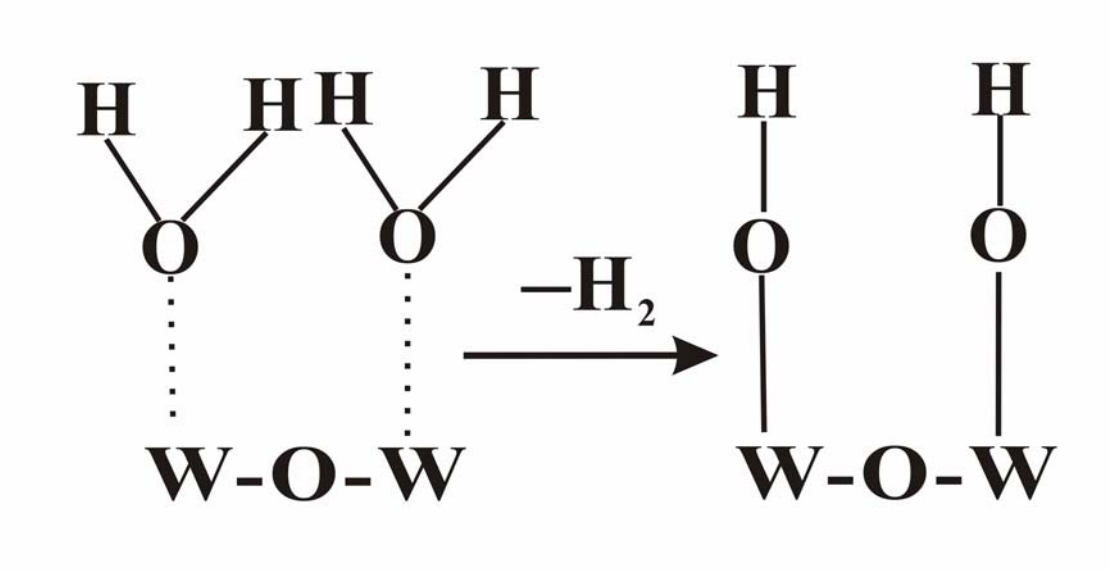

Fig. 11 Schematic of surface water conversion on the WO_3.

Fig. 9d shows the temperature dependence of the WO_3-SnO_2 HNS humidity sensor at various values of RH. Even at low humidity of 11% RH, the humidity sensor showed an increase in resistance as temperature was raised from 24 to 40℃. This probably showed an evidence that much water was adsorbed. It should be noted that the sensor exhibited much higher stability against high temperature under high humidity.

Double Schottky Diode Model is proposed to obtain good understanding the performance of WO_3-SnO_2 HNS humidity sensor. Since, the band gap of WO_3 and SnO_2 at room temperature are about 2.7eV and about 3.6eV [36-37], the work function of WO_3 (4.41eV) is slightly greater in comparison to that of SnO_2 (4.18eV) [38], the energy band structure of the hetero-contact might be configured as that in Fig. 10b. The current through the heterojunction is expressed by [39-40]

$$J = \frac{2J_{S1}J_{S2}sh(\frac{qV}{2k_0T})}{(J_{S1}\exp[\frac{qV}{2k_0T}] + J_{S2}\exp[-\frac{qV}{2k_0T}])}, \quad (2)$$

Where $J_S = A^*T^2\exp(-\frac{\phi}{k_0T})$ is the current-voltage relationship of single Schottky Diode, $A^* = \frac{4\pi q m_n^* k^2}{h^3}$ the effective Richardson constant, q the unit electronic charge, k the Boltzmann constant, T the absolute temperature and the V $(V = V_1 + V_2)$ the voltage applied to the barrier. According to equation (2), the current flowing through the WO_3-SnO_2 heterojunction is determined by the factors of temperature and the height of electrostatic grain boundary barriers of both WO_3 and SnO_2. Below 100℃, the barrier height for either WO_3 or SnO_2 decrease with increasing the humidity due to the increase of electron density on the surface. But at temperature above 100℃，the barrier height of WO_3 increases because of the catalytic reaction. And it make a negative effect on the sensitivity of the humidity sensor. But it can be speculated that when the humidity sensor operate at enough high temperature, extremely little physical adsorbed water can cover the surface, thus the catalytic reaction on the surface of WO_3 become weak. What is more, H_2O reacts with both W lattice and O lattice, similar to SnO_2. As a result, the resistance significantly decreases, as shown in Fig. 9d. As we know, high humidity offers high pressure of water vapor, so higher temperature is need to observe a reduction in the sensor resistance.

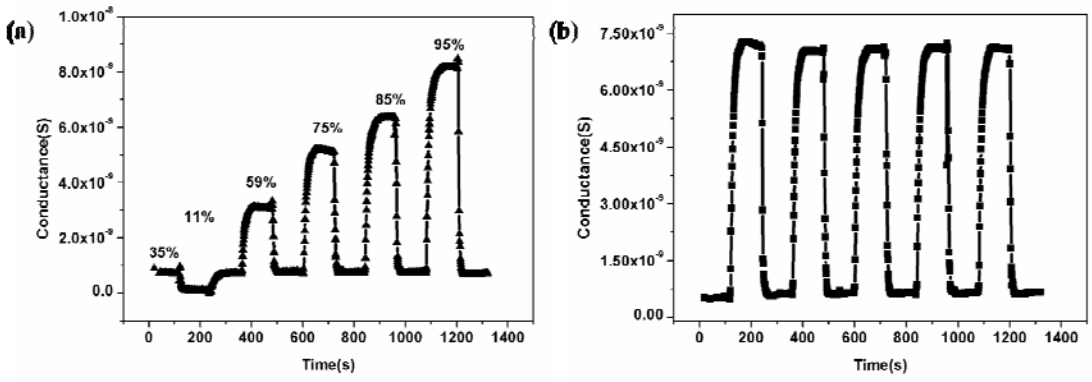

Fig. 12 (a) Typical response curves of WO_3-SnO_2 HNS sensor to various RH at 80℃. (b) Dynamic responsive curves to 98% RH at 80℃.

Dynamic response was measured to further investigate the humidity properties of the WO_3-SnO_2 HNS sensor at high temperature of 80℃. Fig. 12a plots the typical response characteristics towards different RH varying from 11% to 98% RH. It can be seen that the conductance changes rapidly upon exposure to different RH. With increasing RH, the sensitivity greatly increases. Figure 12b shows dynamic characteristics at 98% RH for five cycles. The sensitivity has very slight variation, indicating the stability of the sensor working at high temperature.

To compare the sensing properties of WO_3-SnO_2 HNS sensor working at room temperature and 80℃, important characteristics including stability, sensitivity, response/recovery time had been investigated. Fig. 13a shows the equilibrium conductance of the humidity sensor in the air after testing at various values of RH. The equilibrium

conductance increased when taken out from higher RH to the air, and decreased when it was taken out from lower RH, indicating serious hysteresis working at room temperature. However, when the sensor operated at 80℃, the equilibrium conductance nearly kept as a constant. The ratio of adsorption and desorption of water molecules on the oxide surface was controlled by temperature[29]. And the sensitivity at 80℃ had no significant decrease compared to that of room temperature, as shown in Fig. 13b. What was more, working at 80℃, the sensor showed fast response and rapid recovery at high humidity, as shown in Fig. 13c and Fig. 13d. This may result from fast adsorption and desorption of water molecules at high temperature. But at 11% RH, the sensor showed a longer recovery time at 80℃. This is probably because of the strong bonding of O_2^- with the surface in low humidity, which can only be replaced slowly by water molecules [41].

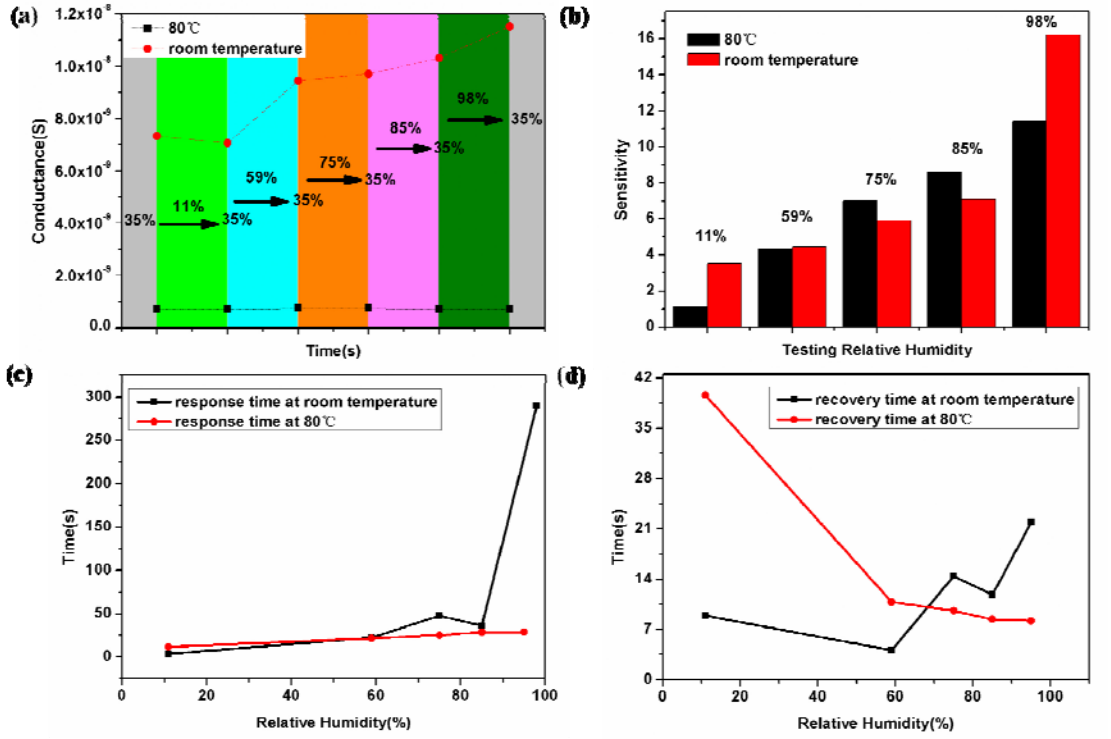

Fig. 13 Characteristic comparison of the WO_3-SnO_2 HNS sensor working at room temperature and 80℃. (a) Equilibrium conductance of the humidity sensor when taken back to the air after testing in relative humidity . (b) The sensitivity against various RH. (c) and (d) Response and recovery times of humidity sensors against various RH.

4 Conclusions

In summary, we developed a facial and green method for synthesis of WO_3-SnO_2 HNS. The test results show that the as prepared hollow spheres exhibits excellent humidity sensing properties at high temperature compared to SnO_2 NPs and WO_3 NPs synthesized by the same method. The humidity sensor can stable work at temperature as high as 80℃. The response time decreased from 289 to 29s, the recovery time reduced from 22 to 8s at 98% RH as the work temperature was raised from 24 to 80℃. The excellent performance of the WO_3-SnO_2 HNS sensors at high temperature indicated a way to develop novel semiconductor humidity sensors with high performances.

Acknowledgements

This work is financially supported by the National Natural Science Foundation of China (Grant no. 61376073).

References

[1] L.T. Chen, C.Y. Lee, and W.H. Cheng, Sens. Actuators, A, 2008, 147, 522-528.

[2] T.L. Yeo, T. Sun, K.T.V. Grattan, Sens. Actuators, A, 2008, 144, 280-295.

[3] X.Q. Fu, C. Wang, H.C. Yu, Y.G. Wang, T.H. Wang, Nanotechnology, 2007, 18, 145503.

[4] A. Zainelabdin, G. Amin, S. Zaman, O. Nur, J. Lu, L. Hultman and M. Willander, J. Mater. Chem., 2012, 22, 11583.

[5] Z. Li, H. Zhang, W. Zheng, W. Wang, H. Huang, C. Wang, A.G. MacDiarmid, Y. Wei, J. Am. Chem. Soc, 2008, 130,5036-5037.

[6] P.M. Faia, C.S. Furtado, A.J. Ferreira, Sens. Actuators, B, 2004, 101, 183-190.

[7] L.L. Gu, K.B. Zhang, Y. Zhou, J. Li, X.L. Mo, G.R. Patzke, G.R. Chen, Sensors and Actuators B, 2011, 159,1-7.

[8] W. Tai, J. Oh, Thin Solid Films， 2002, 422, 220.

[9] W. Tai, J. Kim, J. Oh, Sens. Actuators B, 2003, 96, 477.

[10] R.S. Niranjan, S.D. Sathaye, I.S. Mulla, Sens. Actuators B, 2001, 81, 64.

[11] B.M. Kulwicki, J. Am. Ceram. Soc, 1991, 74, 697-708.

[12] E.R. Leite, I.T. Weber, E. Longo, J.A. Varela, Advanced Materials, 2000, 12, 965-968.

[13] Q. Kuang, C.S. Lao, Z.L. Wang, Z.X. Xie, L.S. Zheng, J.Am.Chem.Soc. 2007, 129, 6070-6071.

[14] L.L. Fields, J.P. Zheng, Y. Cheng and P. Xiong, Appl. Phys. Lett., 2006, 88,263102.

[15] R.Azimirad, N.Naseri, O.Akhavan and A.Z.Moshfegh, J. Phys. D: Appl. Phys. 2007, 40, 1134-1137.

[16] M.Miyauchi, A.Nakajima, T.Watanabe and K.Hashimoto, Chem. Mater. 2002, 14, 2812-2816.

[17] N. Parvatikar, S. Jain, S. Khasim, M. Revansiddappa, S.V. Bhoraskar, M.V.N. Ambika Prasad, Sens. Actuators B, 2006, 114, 599-603.

[18] D. Patil, Y.K. Seo, Y.K. Hwang, J.S. Chang, P. Patil, Sens. Actuators, B, 2008, 132, 116-124.

[19] Z. Ling, and C. Leach, Sens. Actuator B, 2004, 102, 102-106.

[20] Z. Ling, C. Leach and R. Freer, Journal of the European Ceramic Society, 2003, 23, 1881-1891.

[21] Y.P. Ngam, S. Jiemsirilers, S. Supothina, Sensors and Actuators A, 2007, 139, 7-11.

[22] L.L. Wang, Z. Lou, T. Fei, and T. Zhang, J. Mater. Chem, 2012,22, 4767.

[23] X. Chen, Z. Guo, W.H. Xu, H.B. Yao, M.Q. Li, J.H. Liu, X.J. Huang, and S.H. Yu, Adv. Funct. Mater. 2011, 21, 2049-2056.

[24] H.J. Song, X.H. Jia, H. Qi, X.F. Yang, H. Tang, and C.Y. Min, J. Mater. Chem, 2012,22, 3508-3516.

[25] L.L. Wang, T. Fei, J.N. Deng, Z. Lou, R. Wang, T. Zhang, J. Mater. Chem, 2012, 22, 18111-18114.

[26] C.C. Li, L.M. Li, Z.F. Du, H.C. Yu, Y.Y. Xiang, Y. Li, Y. Cai, T.H. Wang, Nanotechnology, 2008, 19, 035501-035504.

[27] P. Manjula, R. Boppella, and S. V. Manorama, ACS Appl. Mater. Interfaces, 2012, 4, 6252-6260.

[28] C.Y. Lee, S.J. Kim, I.S. Hwang, J.H. Lee, Sens. Actuators, B, 2009, 142, 236-242.

[29] K.W. Liu, M. Sakurai, and M. Aono, J. Mater. Chem., 2012, 22, 12882-12887.

[30] J. H. Anderson, and G. A. Parks, J.Phys.Chem., 1968, 72, 3362.

[31] S. Pokhrel, and K. S. Nagaraja, Sens. Actuator B, 2003, 92, 144.

[32] E.W. Thornton, and P.G. Harrison, J. Chem. Soc., Faraday Trans.1, 1975, 71, 461.

[33] T. Kuse, and S. Takahashi, Sens. Actuators B., 2000, 67, 36-42.

[34] G. Heiland, and D. Kohl, in: T. Seiyama (Ed), Chemical sensor technology, vol 1, Kodansha, Tokyo, 1989, p. 15-38.

[35] N.K. Pandey, K. Tiwari, A. Roy, and A. Mishra, Int. J. Appl. Ceram. Technol, 2012, 10, 150-159.

[36] C. Janaky, K. Rajeshwar, N.R. de Tacconi, W. Chanmanee, and M.N. Huda, Catalysis Today, 2013, 199, 53-64.

[37] L. Shi, and H.L. Lin, Langmuir, 2010, 26, 18718-18722.

[38] A. Sharma, M. Tomar, V. Gupta, Sens. Actuator B, 2012, 161, 1114-1118.

[39] W.G. Oldham, A.G. Milnes, Solid State Electron., 1963, 6, 121.

[40] W.G. Oldham, A.G. Milnes, Solid State Electron., 1964, 7, 153.

[41] S.R. Morrison, Sens. Actuator, 1982, 2, 329-341.

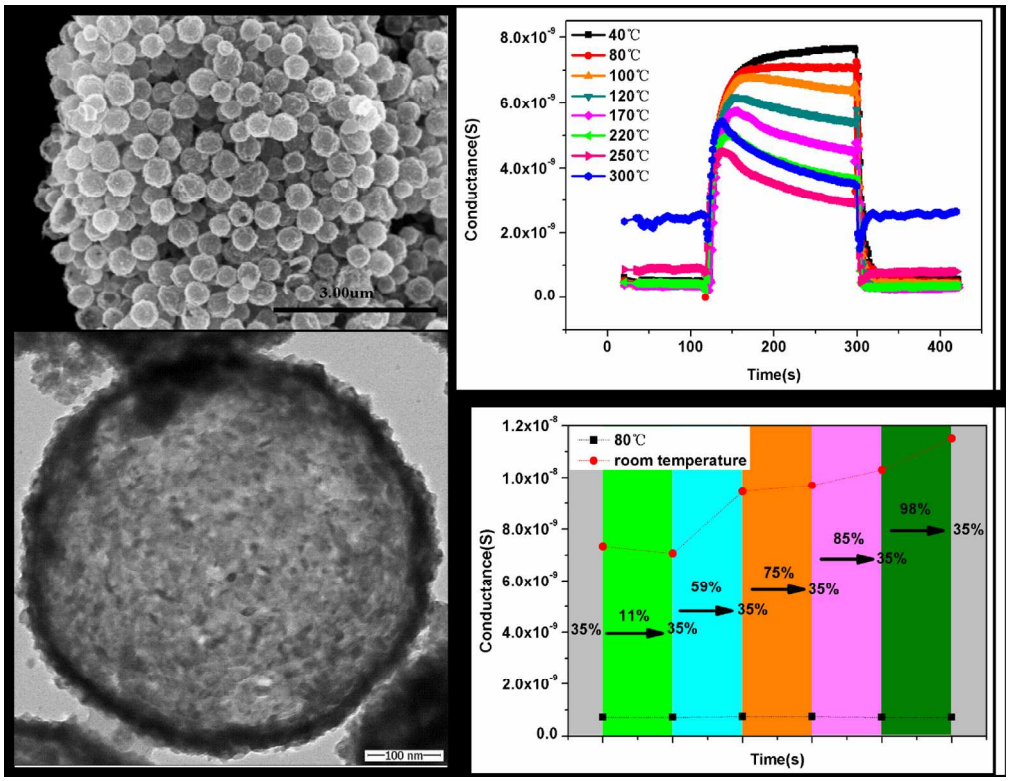

615x474mm (72 x 72 DPI)

We fabricate humidity sensor based on WO_3/SnO_2 composite hollow nanospheres and demonstrate its excellent properties at high temperature.